

A HIGH-PRECESION PSEUDO ARC-LENGTH METHOD WITH POSITIVE VALUE PRESERVATION PROPERTIES BASED ON TV SPLITTING

Chentao Wang¹, Peng Li¹, Leiming He¹, Guozhi Li¹ & Hepeng Dai¹

¹Chinese Aeronautical Establishment, Beijing, China

Abstract

This paper proposed a TV flux splitting scheme based on the complex arc-length coordinate system. By combining the high-precision pseudo arc-length method with the positive-preserving HLL scheme, the robustness of the algorithm is further improved, enabling it to handle complex and extreme cases.

Keywords: high-order, high-precision, Riemann solver, flux splitting

1. Introduction

The hyperbolic conservation law equation is widely used in fields such as implosion dynamics, inertial confinement fusion, computational astronomy, magnetohydrodynamics, computational explosion mechanics, and computational biology. It is extremely difficult to analytically solve the hyperbolic conservation law equation based on continuum mechanics. Currently, only some basic assumptions or latitude reduction are used to simplify the equation, in order to obtain analytical solutions in simple cases. Therefore, using computers for numerical calculations is an effective means of solving such problems.

Accurately numerically solving the hyperbolic conservation law equation remains a challenge, and solving this equation has a clear characteristic that no matter how smooth the initial conditions are, over time, solutions with strong or weak discontinuities (discontinuous functions, discontinuous first-order derivatives) may eventually emerge. The singularity generated during the solving process can pose great challenges to subsequent calculations.

High speed flying aerospace vehicles generate shock waves and sparse waves, and even weak disturbances can cause significant changes in the aircraft. Therefore, efficient, robust, and accurate numerical formats are needed to solve this problem. Therefore, some high-precision and high-resolution numerical formats have been proposed, such as Monotonic Upstream-Centered Scheme for Conservation Laws (MUSCL)[1], Weighted Essentially Non-Oscillatory (WENO)[2, 3, 4], etc. However, when using high-order reconstruction, the numerical solution will generate false oscillations (numerical dispersion) near discontinuities, while when using low-order reconstruction, the numerical solution will be smoothed out at discontinuities (numerical dissipation).

The pseudo arc-length method (PALM)[5] has emerged to address the contradiction between high-precision and high-resolution schemes. The PALM introduces an arc-length parameter and adds an additional constraint equation[6, 7] to adaptively move the spatial grid towards the discontinuity, greatly weakening the singularity at the discontinuity solution. It can be combined with high-precision numerical formats such as WENO to achieve high-resolution capture of large gradient physical quantities. Adaptive grid movement can cause non orthogonality in physical space, which poses great difficulties in constructing high-precision formats. In this paper, through coordinate transformation, the control equation is mapped to the uniformly orthogonal arc-length coordinate system of the grid, and the WENO scheme under the uniform grid algorithm is adopted to improve computational efficiency.

This paper focuses on proposing a high-precision PALM based on Toro-Vázquea (TV)[8] splitting. Existing TV algorithms are mainly based on the original Euler equation[8], and there is still a lack of research on TV splitting algorithms in complex coordinate systems. Therefore, this paper expands the application scope of the TV splitting algorithm and expands its application scope. In addition, to address the problem of negative density and pressure in high-precision numerical formats in arclength coordinate systems (where sound velocity generates imaginary numbers, reducing algorithm robustness and causing calculation termination), a high-precision original operator was combined with a stable Lax Friedrich positive preservation scheme to form a high-precision operator with positive preservation properties and improve the algorithm stability, enabling the algorithm to handle extreme problems such as strong shock waves[9], low density, and low pressure. The calculation results show that the PALM based on TV splitting for the convective flux and the pressure flux has excellent properties, such as long-term calculation without distortion, high calculation accuracy, and strong capture of shock waves and other interruptions. This algorithm has certain guiding significance for fluid dynamics related problems in the aerospace field and can improve computational efficiency.

2. Governing equations

2.1 Euler equations

Consider the 2D Euler equations

$$\frac{\partial \mathbf{U}}{\partial t} + \frac{\partial \mathbf{F}(\mathbf{U})}{\partial x} + \frac{\partial \mathbf{G}(\mathbf{U})}{\partial y} = 0. \tag{1}$$

where

$$\mathbf{U} = \begin{pmatrix} \rho \\ \rho u \\ \rho v \\ \rho E \end{pmatrix}, \mathbf{F}(\mathbf{U}) = \begin{pmatrix} \rho u \\ \rho u^2 + p \\ \rho uv \\ (\rho E + p) u \end{pmatrix}, \mathbf{G}(\mathbf{U}) = \begin{pmatrix} \rho v \\ \rho uv \\ \rho v^2 + p \\ (\rho E + p) v \end{pmatrix}. \tag{2}$$

The ideal gas state equation is as follows

$$\rho E = \rho e + \frac{\rho \left(u^2 + v^2\right)}{2}, \rho e = \frac{p}{\gamma - 1}.$$
(3)

where ρ is the density, u and v are velocity vector components, E is the total energy, p is pressure, e is the internal energy. γ indicates the ratio of specific heat.

2.2 Pseudo arc-length method

The PALM starts from the perspective of eliminating or reducing the singularity of solutions to hyperbolic partial differential equations. By introducing arc-length parameters $\xi = \xi(x,y), \eta = \eta(x,y)$ and adding an additional constraint equations, where

$$(d\xi)^2 = (dx)^2 + \sum_{i=1}^n \lambda_{1i} (dw_i)^2, (d\eta)^2 = (dy)^2 + \sum_{i=1}^n \lambda_{2i} (dw_i)^2.$$
 (4)

In the formula: λ_{1_i} and λ_{2_i} represent weighting coefficients, $d\omega_{1_i}$ and $d\omega_{2_i}$ represent weighted physical quantities, which can be pressure, velocity, density, etc., and n represents the number of weighted variables.

In order to have a clear understanding of the PALM algorithm, Figure(1) and Figure(2) explain the basic principle of the PALM in one and two dimensional space.

Taking one dimension as an example, equation 4 can be further simplified as

$$(d\xi)^{2} = (dx)^{2} + \sum_{i=1}^{n} \lambda_{i} (d\omega_{i})^{2}.$$
 (5)

Then, it can be further obtained that

$$M(x) = \frac{d\xi}{dx} = \frac{1}{\sqrt{1 - \sum_{i=1}^{n} \lambda_i (\frac{\partial \omega_i}{\partial \xi})^2}} = \sqrt{1 + \sum_{i=1}^{n} \lambda_i (\frac{\partial \omega_i}{\partial x})^2}.$$
 (6)

Where M(x) is the arc-length monitor function. From equation (6), it can be seen that when the arclength parameter ξ is constant, the larger the dw_i , the smaller the dx, that is, in the region with a larger physical quantity gradient modulus, the spatial step size of the grid decreases, i.e. the grid adaptively moves towards the discontinuity. The corresponding geometric meaning can be referred in Figure (1), it can be seen that the solution at the strong discontinuity in the original physical space exhibits strong singularity. Due to the adaptive movement of the grid, the generation of non-physical understanding is avoided. Then the solution at the discontinuity becomes a smooth solution, which is the essence and principle of the PALM.

On the other hand, similar conclusions can be reached for two-dimensional space. From Figure(2), it can be seen that due to the adaptive movement of the grid, the original physical space has undergone deformation. Therefore, directly constructing high-order numerical scheme in the coordinate system (x,y) of Figure(2) is more complex and prone to generating ill conditioned equations, which make it very difficult to solve the equation(1). Therefore, considering coordinate transformation, the control equation(1) is mapped to the arc-length coordinate system (ξ,η) . Since the coordinate system (ξ,η) in Figure(2) is uniformly orthogonal, the uniform grid algorithm can be used to construct the high-order scheme.

The governing equations in the arc-length coordinate system are

$$\frac{\partial \widetilde{\mathbf{U}}}{\partial t} + \frac{\partial \widetilde{\mathbf{F}}\left(\widetilde{\mathbf{U}}\right)}{\partial \xi} + \frac{\partial \widetilde{\mathbf{G}}\left(\widetilde{\mathbf{U}}\right)}{\partial \eta} = 0. \tag{7}$$

with

$$\widetilde{\mathbf{U}} = J(\rho, \rho u, \rho v, \rho E)^{T}.$$
(8)

$$\widetilde{\mathbf{F}}\left(\widetilde{\mathbf{U}}\right) = J(\rho U, \rho U u + \xi_{x} p, \rho U v + \xi_{y} p, (\rho E + p) U)^{T}.$$
(9)

$$\widetilde{\mathbf{G}}\left(\widetilde{\mathbf{U}}\right) = J(\rho V, \rho V u + \eta_x p, \rho V v + \eta_y p, (\rho E + p) V)^T.$$
(10)

Where J is the spatial transformation jacobi $\frac{\partial(x,y)}{\partial(\xi,\eta)}$, U and V are inversion speed in arc-length space, with $U=\xi_x u+\xi_y v$ and $V=\eta_x u+\eta_y v$.

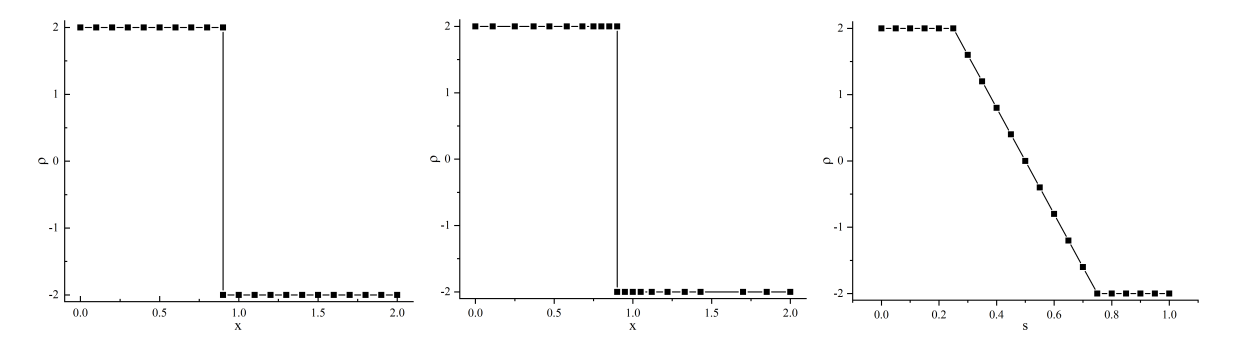


Figure 1 – Principle of 1D PALM (From left to right, they are: original physical space, adaptive physical space, and uniform arc-length space).

2.3 TV splitting

In the flux splitting method, traditional Steger-Warming[10] and Van Leer formats[11] can capture discontinuities corresponding to nonlinear waves, but cannot accurately capture discontinuities corresponding to linear waves, which resulting in excessive dissipation when calculating the contact surfaces and shear waves. In order to combine the advantages of flux difference splitting method and flux vector splitting method, the advection upstream splitting method (AUSM) format has been developed. This paper is based on the Toro-Vázquea (TV) splitting[12] format, which extends the TV splitting from the physical space coordinate system (x,y) to the arc-length coordinate system (ξ,η) .

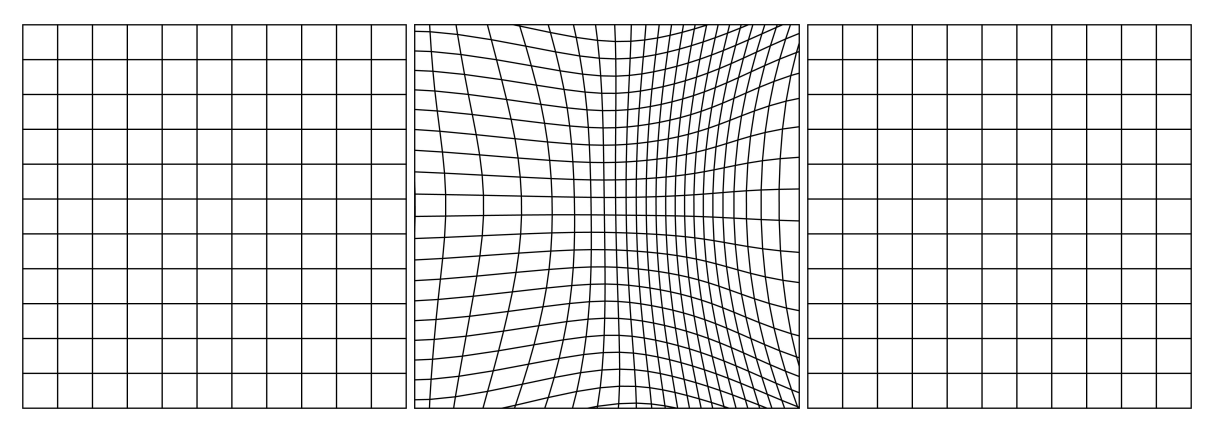


Figure 2 – Principle of 2D PALM (From left to right, they are: original physical space, adaptive physical space, and uniform arc-length space).

Taking the ξ direction as an example, splitting numerical flux $\widetilde{\mathbf{F}}(\widetilde{\mathbf{U}})$ into convective flux $\widetilde{\mathbf{f}_1}(\widetilde{\mathbf{U}})$ and pressure flux $\widetilde{\mathbf{f}_2}(\widetilde{\mathbf{U}})$, where

$$\widetilde{\mathbf{f}}_{1}(\widetilde{\mathbf{U}}) = JU \begin{bmatrix} \rho \\ \rho \mathbf{u} \\ \rho \mathbf{v} \\ \rho \left(u^{2} + v^{2}\right)/2 \end{bmatrix} = JU\mathbf{K}, \widetilde{\mathbf{f}}_{2}(\widetilde{\mathbf{U}}) = J \begin{bmatrix} 0 \\ \xi_{x}p \\ \xi_{y}p \\ U(\rho e + p) \end{bmatrix}. \tag{11}$$

The Jacobi matrices for convective flux and pressure flux are $\widetilde{\mathbf{A}}_1$ and $\widetilde{\mathbf{A}}_2$.

$$\widetilde{\mathbf{A}}_{1} = \frac{\partial \widetilde{\mathbf{f}}_{1}(\widetilde{\mathbf{U}})}{\partial \widetilde{\mathbf{U}}}, \widetilde{\mathbf{A}}_{2} = \frac{\partial \widetilde{\mathbf{f}}_{2}(\widetilde{\mathbf{U}})}{\partial \widetilde{\mathbf{U}}}.$$
(12)

Due to the complexity of matrices $\widetilde{\mathbf{A}}_1$ and $\widetilde{\mathbf{A}}_2$, we can obtain their eigenvalues using Mathematica software, where $\widetilde{\mathbf{A}}_1$ is as follows

$$s = u^2 + v^2. (13)$$

$$\begin{pmatrix}
0 & \xi_{x} & \xi_{y} & 0 \\
-uU & 2u\xi_{x} + v\xi_{y} & u\xi_{y} & 0 \\
-vU & v\xi_{x} & u\xi_{x} + 2v\xi_{y} & 0 \\
-sU & \xi_{x}u^{2} + \xi_{y}uv + \frac{\xi_{x}s}{2} & \frac{\xi_{y}s}{2} + \xi_{x}uv + \xi_{y}v^{2} & 0
\end{pmatrix}.$$
(14)

Then $\widetilde{\mathbf{A}}_2$ is also as follows

$$z = \gamma - 1, \kappa = (2p - \rho sz), c = \sqrt{\gamma \frac{p}{\rho}}.$$
 (15)

$$\begin{pmatrix}
0 & 0 & 0 & 0 \\
\frac{\xi_{x}sz}{2} & -u\xi_{x}z & -v\xi_{x}z & \xi_{x}z \\
\frac{\xi_{y}sz}{2} & -u\xi_{y}z & -v\xi_{y}z & \xi_{y}z \\
-\frac{\gamma U\kappa}{2\rho z} & \frac{\xi_{x}}{z}c^{2} - \gamma uU & \frac{\xi_{y}}{z}c^{2} - \gamma vU & \gamma U
\end{pmatrix}.$$
(16)

Further, the eigenvalues of matrix $\widetilde{\mathbf{A}}_1$ and $\widetilde{\mathbf{A}}_2$ can be obtained as

$$\lambda^{T}_{\widetilde{\mathbf{A}}_{1}} = \begin{bmatrix} 0 \\ U \\ U \\ U \end{bmatrix}, \lambda^{T}_{\widetilde{\mathbf{A}}_{2}} = \begin{bmatrix} \frac{u\xi_{x}}{2} + \frac{v\xi_{y}}{2} - \frac{\sqrt{\frac{\rho u^{2}\xi_{x}^{2} + 2\rho uv\xi_{x}\xi_{y} + \rho v^{2}\xi_{y}^{2} + 4\rho\gamma\xi_{x}^{2} + 4\rho\gamma\xi_{y}^{2}}{\rho}} \\ 0 \\ 0 \\ \frac{u\xi_{x}}{2} + \frac{v\xi_{y}}{2} + \frac{\sqrt{\frac{\rho u^{2}\xi_{x}^{2} + 2\rho uv\xi_{x}\xi_{y} + \rho v^{2}\xi_{y}^{2} + 4\rho\gamma\xi_{x}^{2} + 4\rho\gamma\xi_{y}^{2}}{\rho}} \\ \frac{u\xi_{x}}{2} + \frac{v\xi_{y}}{2} + \frac{\sqrt{\frac{\rho u^{2}\xi_{x}^{2} + 2\rho uv\xi_{x}\xi_{y} + \rho v^{2}\xi_{y}^{2} + 4\rho\gamma\xi_{x}^{2} + 4\rho\gamma\xi_{y}^{2}}{\rho}} \end{bmatrix}.$$
 (17)

Then, by defining the inverse sound velocity in the arc-length space, the characteristic values of pressure flux can be further simplified as

$$\lambda^{T}_{\widetilde{\mathbf{A}}_{2}} = \begin{bmatrix} \frac{1}{2} \left(U - \sqrt{U^{2} + 4C_{\xi}^{2}} \right) \\ 0 \\ \frac{1}{2} \left(U + \sqrt{U^{2} + 4C_{\xi}^{2}} \right) \end{bmatrix}, C_{\xi} = \sqrt{\gamma \frac{p}{\rho} \left(\xi_{x}^{2} + \xi_{y}^{2} \right)}.$$
 (18)

Similarly, the eigenvalues of the Jacobi matrix for η -direction convective flux $\widetilde{\mathbf{g}}_1\left(\widetilde{\mathbf{U}}\right)$ and pressure flux $\widetilde{\mathbf{g}}_2\left(\widetilde{\mathbf{U}}\right)$ can be obtained as

$$\widetilde{\mathbf{B}}_{1} = \frac{\partial \widetilde{\mathbf{g}}_{1}(\widetilde{\mathbf{U}})}{\partial \widetilde{\mathbf{U}}}, \widetilde{\mathbf{B}}_{2} = \frac{\partial \widetilde{\mathbf{g}}_{2}(\widetilde{\mathbf{U}})}{\partial \widetilde{\mathbf{U}}}.$$
(19)

Further, the eigenvalues of $\widetilde{\mathbf{B}}_1$ and $\widetilde{\mathbf{B}}_2$ can be obtained as

$$\lambda^{T}_{\widetilde{\mathbf{B}}_{1}} = \begin{bmatrix} 0 \\ V \\ V \\ V \end{bmatrix}, \lambda^{T}_{\widetilde{\mathbf{B}}_{2}} = \begin{bmatrix} \frac{u\eta_{x}}{2} + \frac{v\eta_{y}}{2} - \frac{\sqrt{\frac{\rho u^{2}\eta_{x}^{2} + 2\rho uv\eta_{x}\eta_{y} + \rho v^{2}\eta_{y}^{2} + 4\rho\gamma\eta_{x}^{2} + 4\rho\gamma\eta_{y}^{2}}{\rho}}}{0} \\ 0 \\ 0 \\ \frac{u\eta_{x}}{2} + \frac{v\eta_{y}}{2} + \frac{\sqrt{\frac{\rho u^{2}\eta_{x}^{2} + 2\rho uv\eta_{x}\eta_{y} + \rho v^{2}\eta_{y}^{2} + 4\rho\gamma\eta_{x}^{2} + 4\rho\gamma\eta_{y}^{2}}{\rho}}}{2} \end{bmatrix}.$$
(20)

Then, the characteristic values of pressure flux can be further simplified as

$$\lambda^{T}_{\widetilde{\mathbf{B}}_{2}} = \begin{bmatrix} \frac{1}{2} \left(V - \sqrt{V^{2} + 4C_{\eta}^{2}} \right) \\ 0 \\ \frac{1}{2} \left(V + \sqrt{V^{2} + 4C_{\eta}^{2}} \right) \end{bmatrix}, C_{\eta} = \sqrt{\gamma \frac{p}{\rho} \left(\eta_{x}^{2} + \eta_{y}^{2} \right)}. \tag{21}$$

For solving numerically equation(7), we adopt a conservative method of the form

$$\widetilde{\mathbf{U}}_{i,j}^{n+1} = \widetilde{\mathbf{U}}_{i,j}^{n} - \frac{\Delta \xi}{\Delta t} \left[\widetilde{\mathbf{F}}_{i+\frac{1}{2},j} - \widetilde{\mathbf{F}}_{i-\frac{1}{2},j} \right] - \frac{\Delta \eta}{\Delta t} \left[\widetilde{\mathbf{G}}_{i,j+\frac{1}{2}} - \widetilde{\mathbf{G}}_{i,j-\frac{1}{2}} \right]. \tag{22}$$

The numerical flux $\widetilde{\mathbf{f}}_{i+\frac{1}{2},j}$ at the half node can be decomposed into the convective flux $\widetilde{\mathbf{f}}_{1_{i+\frac{1}{2},j}}$ and the pressure flux $\widetilde{\mathbf{f}}_{2_{i+\frac{1}{2},j}}$, with

$$\widetilde{\mathbf{F}}_{i+\frac{1}{2},j} = \widetilde{\mathbf{f}}_{1_{i+\frac{1}{k},j}} + \widetilde{\mathbf{f}}_{2_{i+\frac{1}{k},j}}.$$
 (23)

We use the upwind scheme to calculate the convective numerical flux at the midpoint

$$\widetilde{\mathbf{f}}_{1_{i+\frac{1}{2},j}} = \begin{cases} J_{1/2}U_{1/2}\mathbf{K}_{L}, U_{1/2} > 0 \\ J_{1/2}U_{1/2}\mathbf{K}_{R}, U_{1/2} < 0 \end{cases}$$
 (24)

The calculation formula for the pressure numerical flux at the midpoint is as follows

$$\widetilde{\mathbf{f}}_{2_{i+\frac{1}{2},j}} = J_{1/2} p_{1/2}(0, \xi_x, \xi_y, \frac{\gamma}{\gamma - 1} U_{1/2})^T.$$
(25)

The velocity and pressure at the interface are obtained by solving the linear solution of the Riemann problem composed of pressure subsystems

$$U_{1/2} = \frac{\rho_R S_R^M U_R - \rho_L S_L^M U_L - p_R + p_L}{\rho_R S_R^M - \rho_L S_L^M}.$$
 (26)

$$p_{1/2} = \frac{\rho_R S_R^M p_L - \rho_L S_L^M p_R}{\rho_R S_R^M - \rho_L S_L^M} - \frac{\rho_R S_R^M \rho_L S_L^M (U_R - U_L)}{\rho_R S_R^M - \rho_L S_L^M}.$$
 (27)

In equation(26) and equation(27), the wave velocity is calculated using the characteristic value equation(18) of the pressure subsystem, with

$$S_L^M = \frac{1}{2} \left(U - \sqrt{U^2 + 4C_{\xi}^2} \right)_L, S_R^M = \frac{1}{2} \left(U + \sqrt{U^2 + 4C_{\xi}^2} \right)_R.$$
 (28)

2.4 Hybrid TV Riemann solver

Although the TV format can not only accurately capture shock waves, but also contact discontinuities and shear waves, the TV format can generate non-physical understanding of negative density and negative pressure when calculating certain complex problems due to the instability of shock waves. Research has shown that under appropriate wave velocity estimation, the HLL type format automatically satisfies the entropy condition and has positive preservation. Therefore, this paper mixes the HLL format with the TV format to produce a stable and robust composite format.

$$\widetilde{S}_{L}^{M} = \min\left(0, \left(U - C_{\xi}\right)_{L}\right), \widetilde{S}_{R}^{M} = \max\left(0, \left(U + C_{\xi}\right)_{R}\right). \tag{29}$$

$$\widetilde{\mathbf{F}}_{HLL,i+\frac{1}{2},j} = \frac{\widetilde{\mathbf{F}}_L \widetilde{S}_R^M - \widetilde{\mathbf{F}}_R \widetilde{S}_L^M - \widetilde{S}_R^M \widetilde{S}_L^M \left(\widetilde{\mathbf{U}}_L - \widetilde{\mathbf{U}}_R\right)}{\widetilde{S}_R^M - \widetilde{S}_L^M}.$$
(30)

The numerical flux of the mixed format can be expressed as

$$\widetilde{\mathbf{F}}_{TV-HLL} = \mu \widetilde{\mathbf{F}}_{TV} + (1 - \mu) \widetilde{\mathbf{F}}_{HLL}. \tag{31}$$

Where μ is a switching function with values of 0 or 1. A simple and effective strategy is that when the calculation result $\widetilde{\mathbf{U}}^{n+1}$ generates negative density or negative pressure value, μ is set 0, otherwise it is 1.

3. Numerical tests

3.1 2D Sedov blast problem

We consider a very strong explosion wave problem, the calculation region is $[0,1.1] \times [0,1.1]$, the pseudo arc- length control function(6) is $M = \sqrt{1 + \rho^2 + 15 |\nabla \rho|^2}$, and the calculation time is t = 0.001. The lower and left boundaries are set as reflection boundaries, and the right and upper boundaries are set as exit boundaries. The explosion point is set at the origin of the coordinates, the calculated number of grids is 200×200 , and the detailed initial value conditions are as follows:

$$(\rho, u, v, p, \gamma) = \begin{cases} (1, 0, 0, 4 \times 10^{-13}, 1.4) \text{ else} \\ (1, 0, 0, \frac{9.79264}{\Delta x \Delta y} \times 10^4, 1.4) x \le \Delta x, y \le \Delta y \end{cases}$$
(32)

Figure(3) shows the density map of the 2D sedov problem. The flow field in this example contains extremely high pressure ratios and extremely low pressures. If no positive limiters are added during the numerical solution process, it is easy to generate negative pressures due to errors in the numerical format, which can cause the program to terminate prematurely. From the results in Figure(3), it can be seen that the program ran to the final moment under the constraint of the positive limiter and obtained the correct calculation result, indicating that the hybrid limiter proposed in this paper played a positive role, This greatly enhances the robustness and stability of the algorithm. From the calculation results, it can be seen that the density contour lines obtained by the pseudo arc length algorithm are clearer and sharper, and their numerical solutions are on the interface The low dissipation at the discontinuity indicates that the pseudo arc length algorithm has a high resolution in capturing strong shock waves.

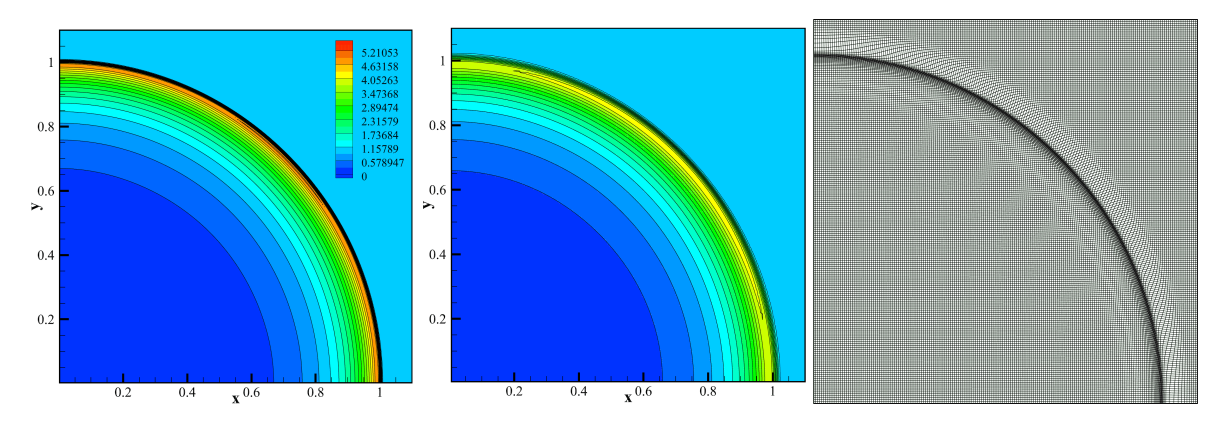


Figure 3 – 2D sedov problem-density. (From left to right, they are: PALM, fixed grid, mesh of PALM)

3.2 Double Mach reflection problem

This is a common calculation example in practical engineering problems, where a shock wave with a Mach number of 10 is directed towards a wedge at a certain angle. By changing the angle of the reference frame, the calculation area of this problem can be set to $[0,4] \times [0,1]$, the number of calculation grids is 640×160 , and the value of the pseudo arc-length control function is $M = \sqrt{1+2|\nabla\rho|^2}$. The calculated termination time is set t=0.2. A Mach number 10 oblique shock wave is directed at a 60 degree angle towards the surface of a wedge-shaped object that coincides with the x-axis, forming a rich flow field structure, such as jets, vortices, shear layers, etc. The initial conditions are as follows:

$$(\rho, u, v, p, \gamma) = \begin{cases} (8, 8.25 \cos \theta, -8.25 \sin \theta, 116.5, 1.4) x < x_0 + \frac{y}{\sqrt{3}} \\ (1.4, 0, 0, 1, 1.4) x \ge x_0 + \frac{y}{\sqrt{3}} \end{cases}$$
 (33)

Figure (4) shows the density map of the Double Mach reflection problem. From the calculation results, it can be seen that the density and pressure contour lines of the PALM based on TV splitting are clearer and sharper, and its numerical solution has lower dissipation at interface discontinuities, indicating that the PALM has higher resolution in capturing strong shock waves. In addition, during the process of solving the physical quantities on both sides of the normal direction of the shock wave surface, it is easy to generate negative density and pressure in numerical calculations due to the instability of the shock wave. The mixed operator enhances the robustness of the algorithm, thus supporting the complete calculation of the program.

3.3 High Mach number astrophysical jets

High Mach number astrophysical jets are typically believed to be generated by processes such as supernova explosions, or star formation. They have extremely high Mach numbers and exhibit complex jet structure. This example considers a jet flow with a Mach number of 2100. The calculation region of this example is $[0,1] \times [-0.25,0.25]$, and the region is initially filled with $(\rho,u,v,p,\gamma) = (0.5,0,0,0.4127,1.667)$. The top, bottom, and right sides are set as outflow boundary conditions, and the left boundary region is set with inflow boundary conditions, specifically:

$$(\rho, u, v, p, \gamma) = \begin{cases} (5,800, 0, 0.4127, 1.667), -0.05 \le y \le 0.05 \\ (5,0,0,0.4127, 1.667), else \end{cases}$$
 (34)

The number of calculation grids is 400×200 , and the value of the pseudo arc-length control function is $M = \sqrt{1+20|\nabla\rho|^2}$. The calculated termination time is set t=0.001. Figure(5) shows the detailed calculation results. This example has a very high requirement for the stability of the algorithm. The head and tail of the jet and the outer boundary of the whole jet are filled with extremely strong shock waves, and the small disturbance will produce negative density and pressure and then suspend the calculation. As can be seen from the calculation results in Figure(5), the algorithm proposed in this paper is very robust and effective, and it can guarantee the calculation to the end time stably. In addition, the pseudo-arc length method maintains a very high resolution due to the adaptive movement

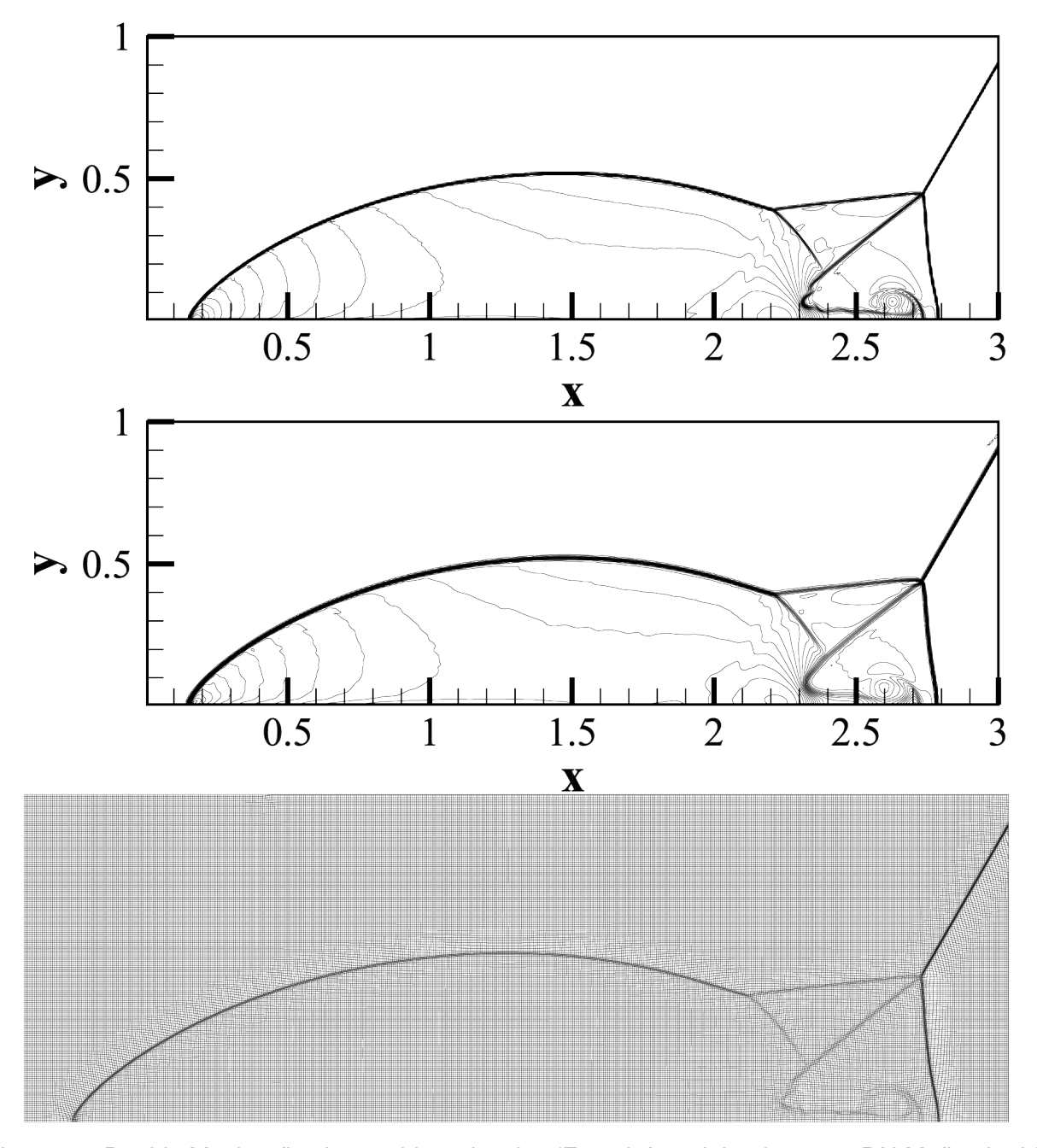


Figure 4 – Double Mach reflection problem-density. (From left to right, they are: PALM, fixed grid, mesh of PALM)

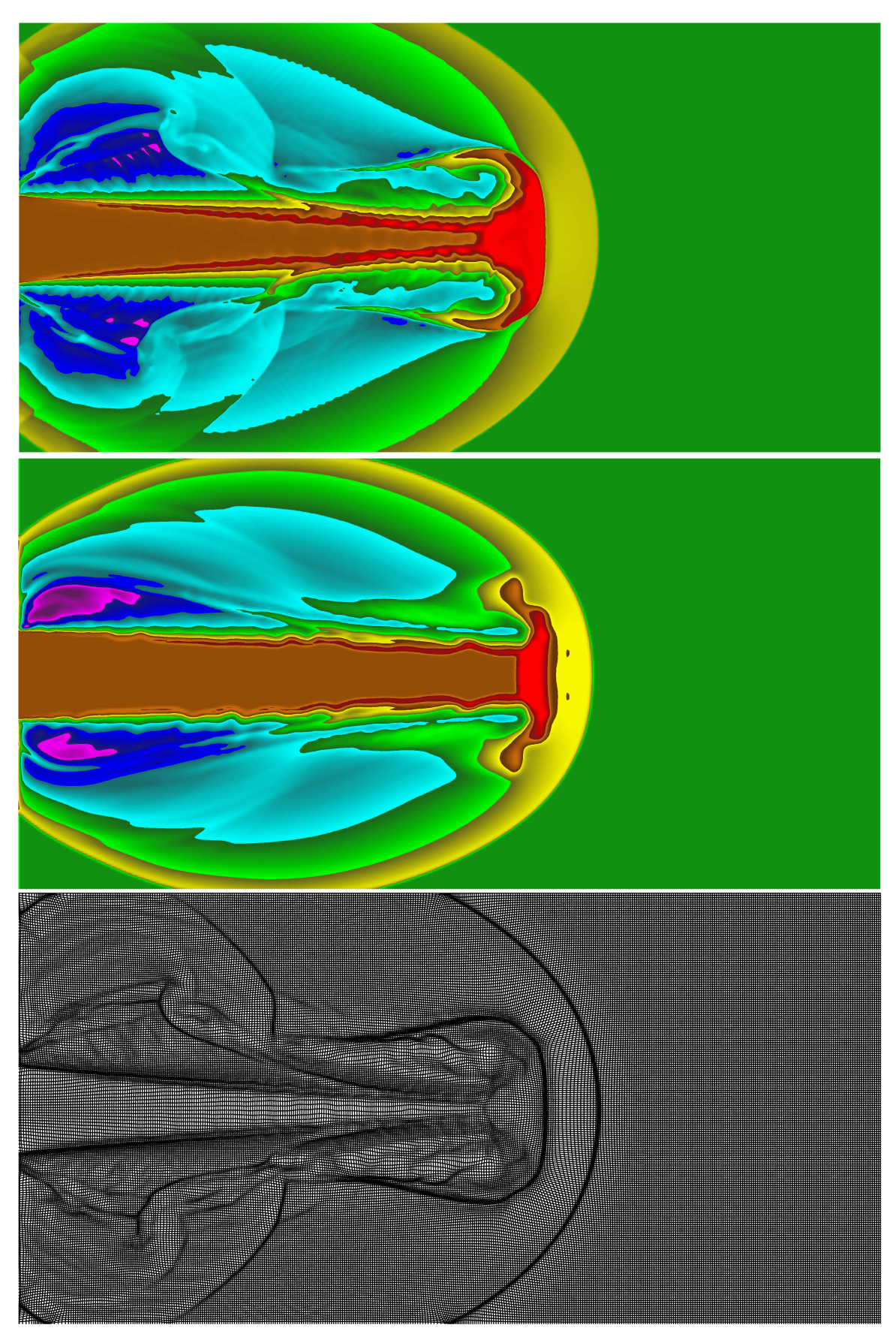


Figure 5 – High Mach number astrophysical jets problem-density. (From left to right, they are: PALM, fixed grid, mesh of PALM)

of the grid, and can obtain a sharp shock surface, which is very advantageous in the calculation of strong shock waves.

4. Concluding Remarks

This paper aims to construct a flux scheme with high-resolution and robust numerical stability. The main work includes: (1) proposed a TV splitting scheme based on the complex arc-length coordinate systems. By decomposing the flux vector into convective flux and pressure flux, the TV splitting is extended from the fixed grid to the complex coordinate system; (2) Mapping non-physical space to arc-length space through coordinate transformation facilitates the construction of high-precision numerical scheme; (3) The calculation results show that the solver constructed in this paper not only has higher accuracy but also effectively overcomes numerical instability in strong shock wave simulation. The application of the numerical format constructed in this paper to complex flow problems such as compressible turbulence, as well as the development of solvers on three-dimensional spatial and unstructured grids, it is worth further research in the future.

5. Contact Author Email Address

Chentao Wang: 615555140@gg.com

6. Copyright Statement

The authors confirm that they, and/or their company or organization, hold copyright on all of the original material included in this paper. The authors also confirm that they have obtained permission, from the copyright holder of any third party material included in this paper, to publish it as part of their paper. The authors confirm that they give permission, or have obtained permission from the copyright holder of this paper, for the publication and distribution of this paper as part of the ICAS proceedings or as individual off-prints from the proceedings.

References

- [1] Zhao J, Hinkelmann R, Liang D, et al. Improved multislope MUSCL reconstruction on unstructured grids for shallow water equations. *International journal for numerical methods in fluids*, 2021, 87:73.
- [2] Gao Z, Fang L, Wang B, et al. Seventh and ninth orders characteristic-wise alternative WENO finite difference schemes for hyperbolic conservation laws. *Computers & Fluids*, 2020, 202:104519.
- [3] Zhao Z, Zhang M. Well-balanced fifth-order finite difference Hermite WENO scheme for the shallow water equations. *Journal of Computational Physics*, 2023, 475:111860.
- [4] Zhang Y, Deng W, Zhu J. A new sixth-order finite difference WENO scheme for fractional differential equations. *Journal of Scientific Computing*, 2021, 87:73.
- [5] Ma T, Wang C, Xu X. Conservative high precision pseudo arc-length method for strong discontinuity of detonation wave. *Applied Mathematics and Mechanics (English Edition)*, 2022, 43(3): 417-436.
- [6] Yuan X, Ning J, Ma T, et al. Stability of newton tvd rungekutta scheme for one-dimensional euler equations with adaptive mesh. *Applied Mathematics and Computation*, 2016, 282: 1-16.
- [7] Yuan X, Ning J, Ma T, et al. Positivity-preserving moving mesh scheme for two-step reaction model in two dimensions. *Computers & Fluids*, 2015, 123: 72-86.
- [8] Toro E, Vázquea-Cendon M. Flux splitting schemes for the Euler equations. *Computers & Fluids*, 2012, 70: 1-12.
- [9] Tang L, Song S, Zhang H. High-order maximum-principle-preserving and positivity-preserving weighted compact nonlinear schemes for hyperbolic conservation laws. *Applied Mathematics and Mechanics (English Edition)*, 2020, 41(1): 173192.
- [10] Steger J, Warming L. Flux vector splitting of the inviscid gasdynamic equations with application to finite-difference methods. *Journal of Computational Physics*, 1981, 40: 263-293.
- [11] Anderson W, Thomas J, Leer B. Comparison of Finite Volume Flux Vector Splittings for the Euler Equations. *AIAA Journal*, 2015, 24: 1453-1460.
- [12] Toro E, Vázquez-Cendón M. Flux splitting schemes for the Euler equations. *Computers & Fluids*, 2012, 70: 1-12.